Enhanced Catalytic Performance of ZnO/Carbon Materials in the Green Synthesis of Poly-substituted Quinolines

Marina Godino-Ojer [a]*, Sergio Morales-Torres [b], Elena Pérez-Mayoral [c]*, Francisco J. Maldonado-Hódar [b]

[a]Facultad de Ciencias Experimentales, Universidad Francisco de Vitoria, UFV, Ctra. Pozuelo-Majadahonda km 1.800, 28223 Pozuelo de Alarcón, Madrid, Spain

[b]Departamento de Química Inorgánica, Facultad de Ciencias, Universidad de Granada, 18071 Granada, Spain

[c]Departamento de Química Inorgánica y Química Técnica, Universidad Nacional de Educación a Distancia, UNED, Facultad de Ciencias, Urbanización Monte Rozas, Avda. Esparta s/n Ctra. de Las Rozas al Escorial Km 5, 528232 Las Rozas – Madrid, Spain

* Corresponding authors:

Elena Pérez Mayoral; eperez@ccia.uned.es
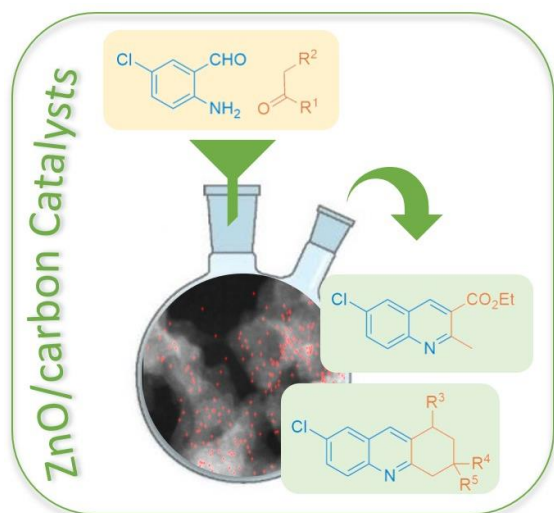
Phone   (+34) 91 398 9047; Fax (+34) 91 398 6697

Marina Godino-Ojer; marina.godino@ufv.es

Abstract

A highly efficient methodology for the selective synthesis of nitrogen heterocycles *via* Friedländer reaction using carbon materials supported ZnO catalysts under the green chemistry domain is presented. The influence of the physicochemical properties of different carbon supports, in particular an activated carbon (AC), multi-walled carbon nanotubes (MWCNT) and a carbon aerogel (CA), on the catalytic performance is discussed. The developed catalysts are easily prepared by simple incipient wetness impregnation and a subsequent thermal treatment. These ZnO/carbon catalysts showed a great performance in the Friedländer condensation of 2-amino-5-chlorobenzaldehyde and carbonylic compounds with enolizable hydrogens, under solvent-free and mild conditions, affording in all cases selectively a total conversion to the corresponding quinoline. Both the Zn loading in combination with the developed microporosity of the selected carbon supports seem to be the key factors determining the catalytic performance. Yields obtained with ZnO/carbon composites prepared are superior to those obtained by others widely used in fine chemistry such as, Zn-catalysts supported on mesoporous silica (SBA-15) and Zn-metal-organic-frameworks (MOF).

36   **Graphical abstract**

37

38

41

1. Introduction
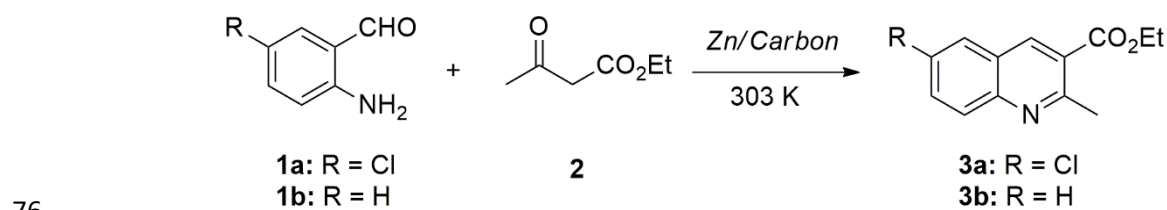
Sustainable Development Goals (SDGs) integrate relevant chemistry challenges opening opportunities for new, green and sustainable chemical research and practices. Cleaner production, preventing the production of wastes, but improving the use of the energy, water and resources, among others, is essential to protect the planet, the societies becoming more sustainable. In this context, the development of sustainable catalytic materials applied to the eco-friendly and efficient fine chemical synthesis is a highly relevant issue.

Zinc oxide (ZnO), occurring in a great variety of nanostructures including nanoparticles, nanorods, nanowires, nanotubes or polyhedral cages has been widely applied in many research fields due to its exceptional and wide range of physicochemical properties. ZnO possesses unique properties such as, a high chemical stability, acid-base character, porosity depending on its different morphology, a broad radiation absorption range, and high photo-stability. These nanostructures are useful on the development of advanced optoelectronics, solar cell, gas sensors, flexible hybrid nanoceramics and in biomedicine, among other applications [1]. Nano-ZnO has been also explored in environmental catalysis because it is cheap, commercially available, biosafe and biocompatible. Nano-ZnO has been also reported as an interesting catalyst for diverse organic transformations, with especial emphasis in the synthesis of relevant biologically active heterocyclic systems [2].

On the other hand, nanostructured carbon materials have attracted a great attention in catalysis due to their unique physicochemical properties. In fact, ZnO/carbon-derived composites have been studied extensively in recent years, because of the synergetic effect between both materials, which has been widely described to improve the catalytic activity of each material by separately. As examples, emitters based on graphene hybrid composites [3]

65   and advanced supercapacitors using activated carbons (ACs) and carbon aerogels (CAs) [4]

66   have been investigated. In addition, an amphiphilic nanocomposite consisting of reduced

67   graphene oxide (rGO), in which ZnO is loaded using polyvinylpyrrolidone (PVP) as an

68   intermediate, followed by *in situ* photoreduction [5], was successfully applied in the synthesis

69   of 3-substituted indoles in water medium [6]. Recently, carbon/ZnO hybrids have been also

70   reported for the synthesis of fine chemicals such as β-acetamido-β-(phenyl)propiophenone

71   [7] and benzimidazoles [8].

72   In this context, the goal of this work is the development of a new methodology for the

73   green synthesis of quinolines, *via* Friedländer reaction, from 2-amino-5-chlorobenzaldehyde

74   **1a** and ethyl acetoacetate **2**, under solvent-free conditions (Scheme 1) exploring for that,

75   novel, efficient, cheap and sustainable ZnO/carbon catalysts.

1a: R = Cl
1b: R = H

2

3a: R = Cl
3b: R = H

76

77   **Scheme 1.** Synthesis of quinolines **3** from 2-amino-5-chlorobenzaldehyde **1** and ethyl

78   acetoacetate **2** catalyzed by ZnO/carbon catalysts.

79   Although different synthetic approaches for the preparation of quinolines **3** and

80   analogues have been reported [9-10], Friedländer reaction consists of the simplest synthetic

81   approach to produce poly-substituted quinolines, a type of nitrogen-containing heterocycles

82   especially interesting due to their therapeutic uses, through cascade reactions with high atom

83   economy [11]. It is important to note that Friedländer reaction is a substrate-dependent

84   condensation [12]. In this work, we synthesized the quinoline **3a**, an analogue of **3b** (Scheme

85   1) as biologically active compound, from 2-amino-5-chlorobenzaldehyde **1a** because this

substrate is commercial, cheaper and more stable than the corresponding 2-aminobenzaldehyde **1b**. Quinoline **3b** is known as histone acetyltransferase (HAT) inhibitor [13-14] but also useful in the synthesis of lavendamycin analogue [15].

Compound **3b** is often obtained using piperidine in hydroalcoholic solutions. Different porous catalysts exhibiting acid or basic properties or even acting as bifunctional catalysts, active in the synthesis of quinoline **3a**, through Friedländer reaction, from mesoporous silicas, metal-organic frameworks to porous carbons as metal-free but also metal-supporting porous carbons have been reported (see supporting information, Table 1S). Considering all of them, carbon catalysts emerge as an interesting alternative to functionalized mesoporous silicas or MOFs due to their easy preparation, high stability and enhanced catalytic performance. While mesoporous silica or CuBTC worked at higher temperature, in general, carbon catalysts yielded similar or notably improved conversions to quinolines, even operating at lower temperature, in the presence of a notable increase of reactants amounts and shorter reaction times. Among the explored carbon materials, metal-free carbons are able to catalyze the reaction affording the corresponding quinoline **3a** in low yields whereas metals supporting carbon materials, particularly cobalt catalysts in which cobalt is as its metallic [16] form or even as CoO [17] in both cases improved the conversion values. Although cobalt has a biologically importance as metal constituent of vitamin B12, excessive exposure can induce adverse health effects [18]. In this context, since nano-ZnO was reported in the synthesis of a great variety of fine chemicals as environmentally benign and non-toxic catalysts, among them biologically heterocyclic systems [2], also considering the unique properties of ZnO, as mentioned above, it is reasonable to think that the combination of both ZnO and porous carbons will allow to obtain new series of biocompatible catalysts for the synthesis of quinoline **3a**.

ZnO/carbon nanocomposites reported herein are easily prepared from carbon supports of our choice showing different textural properties and compositions − commercial AC (Norit RX3), multi-walled carbon nanotubes and 3D-CA prepared in our lab −. Considering that the carbon surface and even the functionalities influence the dispersion and accessibility of the metallic phase, and therefore, the catalytic performance, we selected a microporous carbon (Norit RX 3 AC) and two mesoporous carbon samples comprising oxidized multi-walled carbon nanotubes and a pure carbon aerogel prepared by polymerization of resorcinol–formaldehyde (R–F). All samples were impregnated with aqueous solutions of the corresponding metallic salt to obtain a metal loading of 1 or 3 wt.% and subsequently submitted to thermal treatment, for comparison with CoO samples previously reported [17].

Summarising, these ZnO/carbon catalysts have been found to be highly efficient in the green synthesis of quinolines, from of 2-amino-5-chlorobenzaldehyde **2** and different carbonylic compounds, with enolizable hydrogens at position α-, under mild and solvent-free conditions, notably demonstrating superior catalytic performance than others commercially available Zn-based catalysts, such as Basolite® Z1200, i.e., a MOF with Zn^{II} metal centres, Zn-catalysts supported on mesoporous SBA-15 silica and other carbon catalysts previously reported (Table 1S).

2. Experimental

2.1. Synthesis and characterization of the materials

Three different carbon materials were used as supports: (i) a commercial AC sample from NORIT Nederland B.V. (Norit RX3, labelled hereafter as sample Norit), (ii) multi-walled carbon nanotubes (sample CNT) purchased to Sigma-Aldrich, and (iii) a home-made CA (sample B_{500})

133 synthesized from the polymerization of resorcinol (R) and formaldehyde (F) and posterior

134 carbonization at 773 K [19]. While the Norit AC and the B_{500} CA were used without any

135 chemical treatment, the CNT sample was firstly oxidized by boiling with HNO_3, denoted as

136 CNT_{ox} [20]. Before metal-impregnation carbon supports were milled and sieved to a particle

137 size below 0.25 mm.

138 ZnO/carbon catalysts were prepared by impregnation of the different types of carbon

139 materials (5 g), i.e., Norit, B_{500} and CNT_{ox}, with concentrated aqueous solutions of

140 $Zn(NO_3)_2 \cdot 6H_2O$ to obtain a metal loading of 1 or 3 wt.%. After drying overnight at 383 K, the

141 samples were pre-treated for 2 h under a He flow at 623 K.

142 Three catalyst series were denoted as $CNT_{ox}YZn$, NoritYZn and $B_{500}YZn$, in which "Y" is the

143 theoretical Zn loading expressed as wt.%. Additionally, another catalyst supported on

144 mesoporous SBA-15 silica (SBA15-3Zn), also prepared in our laboratories following a similar

145 procedure [21], and the commercial MOF Basolite® Z1200 (Merck, CAS Number 59061-53-9)

146 were used for comparison purposes.

147 The textural characteristics of the samples were determined by physical adsorption of N_2

148 at 77 K, after outgassing samples overnight at 383 K under high vacuum (10^{-6} mbar). BET

149 surface area (S_{BET}) and micropore volume (W_0) were calculated by applying, respectively, the

150 BET or Dubinin–Radushkevich (DR) equations to the isotherms [22], while mean micropore

151 width (L_0) was determined by Stoeckli equation. The total pore volume (V_T) is defined as the

152 volume of the adsorbed nitrogen at a relative pressure $P/P_0 = 0.95$ [23], and the mesopore

153 volume (V_{meso}) from the difference between V_T and the volume of N_2 adsorbed at $P/P = 0.40$,

154 following the Gurvich rule.

155 The metal content of the catalysts was analysed by Inductively Coupled Plasma (ICP) and

156 by thermogravimetric analyses. The chemical nature and dispersion of the metal were

157 investigated by X-ray diffraction (XRD) using a Phillips PW1710 diffractometer. High resolution

158 transmission microscopy (HRTEM) images were obtained using a Titan FEI G2 microscope. X-

159 ray photoemission spectra (XPS) were recorded using a Kratos Axis Ultra-DLD spectrometer to

160 determine the surface composition of catalysts. This instrument utilizes Mg Kα (1253.6 eV) as

161 the radiation source and a hemispheric electron analyser operating at 12 kV and 10 mA. Survey

162 and multi-region spectra were recorded at C1s, O1s, and Zn2p photoelectron peaks, and each

163 spectral region scanned until good signal-to-noise ratios were achieved.

164 *2.2. Catalytic performance*

165 A mixture of the corresponding 2-amino-5-chlrorobenzaldehyde **1** (2 mmol) and ethyl

166 acetoacetate **2** (5 mmol) in a three-necked vessel, equipped with reflux condenser, septum

167 and thermometer, was placed on a multiexperiment workstation StarFish (Radley's Discovery

168 Technologies, UK). When the temperature reaches 303 K, the catalyst was added (25 mg) and

169 the reaction mixture was stirred for 240 min. The samples were periodically obtained at 15,

170 30, 60, 120, 180 and 240 min and diluted with ethyl acetate (0.5 mL). Subsequently, the

171 catalyst was filtered off and the solvent evaporated in vacuo. The reactions were qualitative

172 analyzed by TLC chromatography performed on a DC-Aulofolien/Kieselgel 60 F_{245} (Merck)

173 using mixtures of CH_2Cl_2/EtOH 98:2 as an eluent. The products were characterized by ^1H NMR

174 spectroscopy. Solution NMR spectra were recorded on a Bruker XRD400 (9.4 Tesla, 400.13

175 MHz for ^1H) spectrometer with a 5-mm inverse-detection H-X probe equipped with a z-

176 gradient coil, at 300K. Chemical shifts (δ in ppm) are given from internal solvent, [d_6] DMSO

177 2.5 for ^1H.

178 Yield (or conversion values) is defined as the fraction of reactant **1** transformed at each

179 reaction time into compounds determined by ^1H NMR. The reactions under study yielded
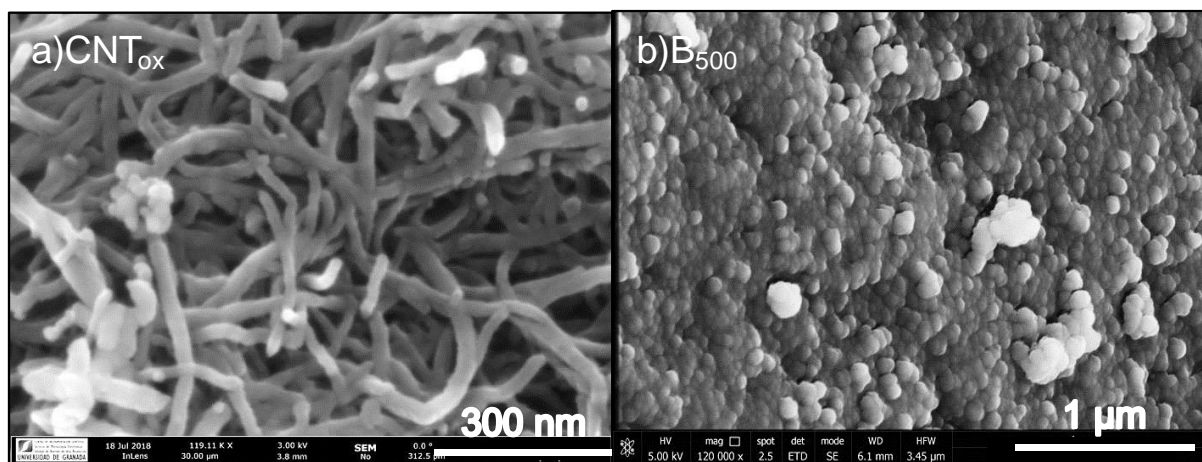
9

180 exclusively the corresponding quinoline, therefore, selectivity being 100 %. Characterization

181 data of quinolines **3** and **5** are in good agreement with those previously reported [24,25].

182 **3.   Results and discussion**

183 *3.1. Characterization of the materials*

184 The selection of the carbon supports from commercial AC, pure carbon gel [19] to

185 functionalized CNTs, providing a wide variety of both textural, morphological, and chemical

186 properties is motivated by our own experience and other authors actively investigating with

187 this type of carbon materials for the Friedländer reaction, as above mentioned, and other fine

188 chemicals synthesis [26, 27]. Nevertheless, other inorganic solids such as a commercial Zn-

189 based MOF (Basolite® Z1200) and Zn-catalyst supported on mesoporous silica (SBA-15) have

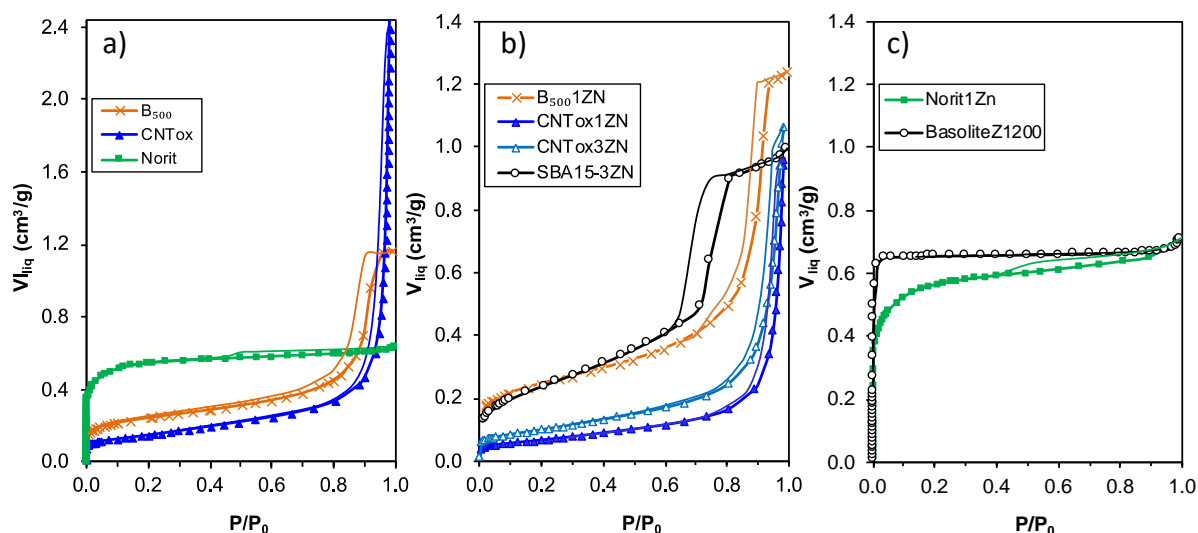190 been also investigated for further comparisons.

191 In this sense, in Figure 1 are showed the SEM images of two selected nanocarbons, as an

192 example. The morphology of the CNT_{ox} support presents a high crosslinking between them

193 forming large bundles of carbon nanotubes (Fig. 1a), while B_{500} showed the typical

194 nanostructure of carbon gels based on the 3D-overlapping of more or less spherical carbon

195 nanoparticles also called primary particles (Fig. 1b).

196

197   **Figure 1.** SEM images of a) CNT_{ox} and b) B_{500} carbon aerogel used as Zn-supports.

198   The nature, morphology and treatments of the supports evidently define the

199   physicochemical properties of their derivative catalysts. In this work, besides to study the

200   ZnO/carbon catalysts, it is also analyzed the properties and performance of MOF Basolite®

201   Z1200 and silica supported catalysts, SBA-3Zn, as anticipated. In this context, the N_2-

202   adsorption isotherms obtained are compared in Figure 2 and the corresponding textural

203   parameters are summarized in Table 1. At a glance, it is pointed out two types of supports

204   (catalysts). Both commercial AC Norit and MOF Basolite® Z1200 are microporous samples

205   showing isotherms type I (Fig 1a and c, respectively), while CNT_{ox}, B_{500} and SBA-15 present

206   isotherms type IV corresponding to mesoporous solids (Fig 1a and b, respectively. Basolite®

207   Z1200 presents the highest microporosity and BET surface area (S_{BET}) values. The straight

208   shape of the isotherm denotes the homogeneity of theses micropores, while the large neck at

209   low P/P_0 observed in the isotherm of the Norit sample pointed out a great heterogeneity of

210   the micropore range. The DR analysis of the isotherms [22] allows determining a mean

211   micropore size (L_0) confirming the narrower microporosity of MOF regarding carbon supports.

212   Microporous samples present the highest S_{BET} values), as expected. The mesoporosity is

213   negligible for the MOF sample, but the isotherm of AC Norit showed a small hysteresis cycle

214   from $P/P_0 > 0.4$.

Figure 2. N_2 adsorption isotherms of a) carbon supports, b) mesoporous catalysts and c) microporous catalysts.

CNT_{ox} presents a scarce microporosity accessible to N_2, but the formation of carbon nanotube bundles generates a high mesopore volume as interparticle spaces. This is pointed out by the small adsorption of N_2 at low relative pressure and the increased adsorption at high P/P_0 values (Fig. 2b). Carbon aerogels present a bimodal pore size distribution, showing an important microporosity formed by intraparticle during carbonization [28], while mesopores are formed again between the primary spherical particles. Thus, the B_{500} support shows a significantly high surface area and mesoporosity (Table 1). When comparing the porosity of supports and catalysts, it is observed that the Zn nanoparticles are blocking partially the porosity, decreasing also the S_{BET} values. The pore volume and the micropore size slowly increased in the catalysts regarding the supports, namely for B_{500} and Norit, which can be related with a small gasification of the support during the decomposition of the nitrate precursors.

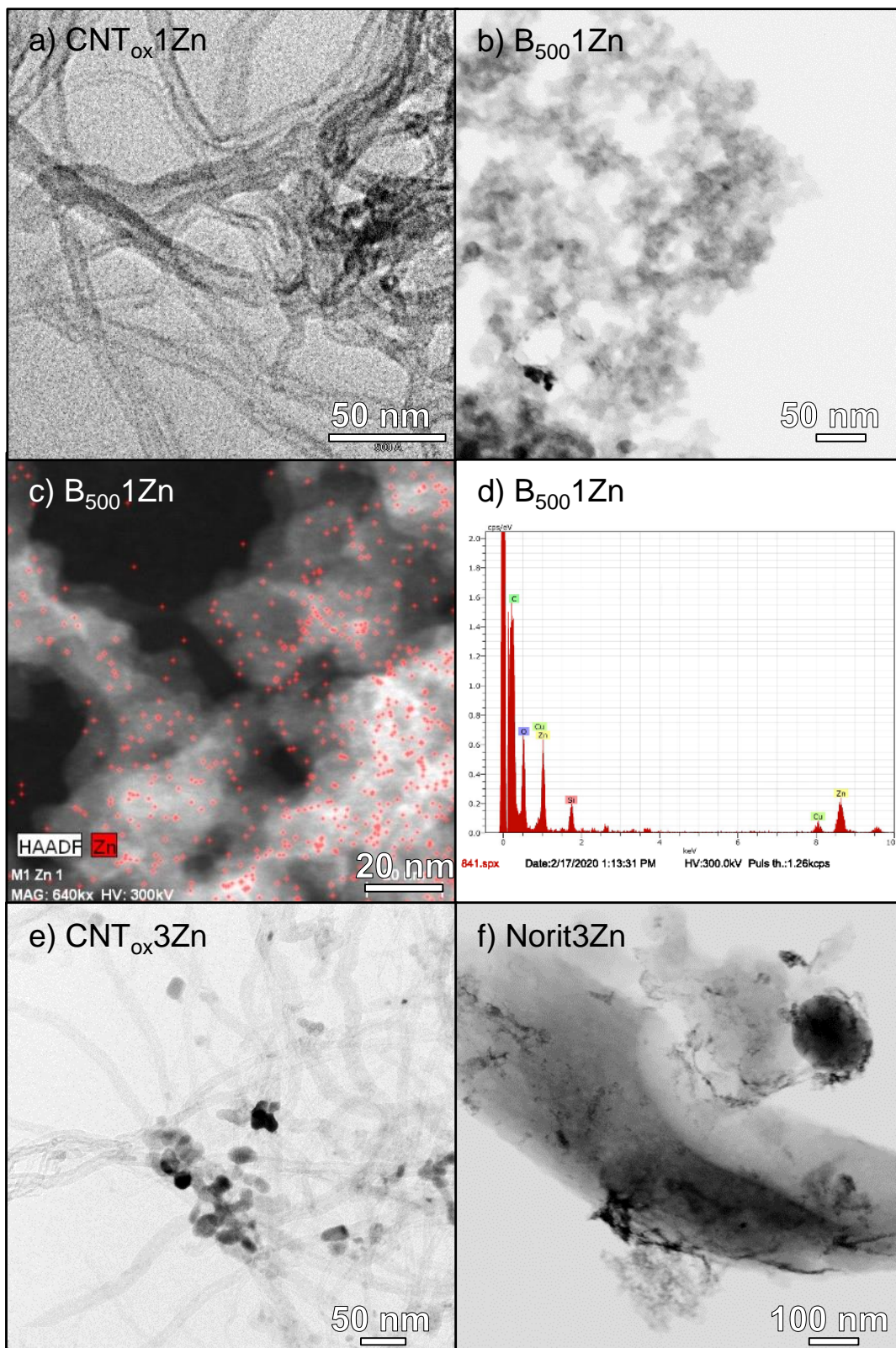**Table 1.** Textural properties of supports and catalysts determined by N_2-adsorption.

Sample	S_{BET} m^2 g^{-1}	W_0 cm^3 g^{-1}	L_0 nm	V_{meso} cm^3 g^{-1}	V_{pore} cm^3 g^{-1}	S_{BJH} m^2 g^{-1}	d_{pore} nm
Norit	1295	0.52	1.3	0.05	0.61	218	39
Norit1Zn	1128	0.55	1.4	0.10	0.69	155	37
CNT$_{ox}$	318	0.14	1.7	0.51	0.71	367	394
CNT$_{ox}$1Zn	151	0.06	1.6	0.33	0.42	183	364
CNT$_{ox}$3Zn	223	0.09	1.6	0.37	0.51	259	358
B$_{500}$	555	0.20	1.5	0.85	1.16	627	10
B$_{500}$1Zn	568	0.24	1.8	0.92	1.22	287	17
Basolite® Z1200	1690	0.65	0.7	0.00	0.68	27	39
SBA15-3Zn	523	0.22	2.0	0.65	0.96	681	7

The identification and quantification of the Zn-phases was carried out by applying different techniques. Commercial Basolite® Z1200 corresponds to the 2-methylimidazole zinc salt ($C_8H_{10}N_4Zn$), therefore with a theoretical Zn content of 2.5 wt.%. The ICP experiments confirmed that the Zn content corresponds to the theoretical content, being 1.0 and 2.8 wt.% for CNT$_{ox}$1Zn and CNT$_{ox}$3Zn samples, respectively. When supported on the microporous Norit sample, the Zn content determined was 1.2 wt.% for Norit1Zn.

The distribution of the metallic phase on the different supports was analyzed by HRTEM (Fig. 3). Small Zn-nanoparticles are difficult to be observed in catalysts prepared at low Zn-loading, (Figs. 3a and b). However, the Zn-mapping and EDX analysis showed a ubiquitous distribution of Zn nanoparticles on the highly porous structure of the B$_{500}$ support (Figs. 3c and
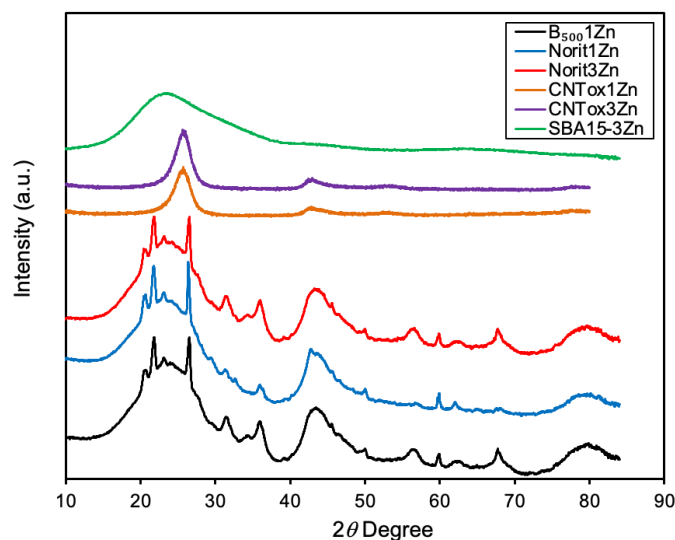
244   d, respectively). Different Zn-nanostructures are observed with increasing the metal loading.

245   Thus, metal Zn nanoparticles are observed between CNT bundles (Fig. 3e), while the metallic

246   phase is forming filamentous structures surrounding support AC Norit (Fig. 3f).

247

248　　　**Figure 3.** HRTEM images of the different Zn-carbon catalysts. Zn-mapping and EDX

249　　　analysis are also included for $B_{500}1Zn$, as examples.

250　　　XRD-patterns for the different catalysts are collected in Figure 4. No diffraction peaks

251　　　corresponding to the metallic phase were observed for catalysts supported on SBA15 or CNT_{ox},

252　　　even at high metal loading. In spite that most of the nanoparticles observed by TEM on

253　　　$CNT_{ox}3Zn$ are very small (between 3-5 nm), some of them present a size between 10-20 nm

254　　　(Fig. 3e), i.e., present a particle size enough to be detected by XRD, which probably can

255　　　indicate a low concentration of these larger nanoparticles or even a high amorphous character

256　　　of these metallic nanostructures (Fig. 4). However, using both B_{500} or Norit supports, the

257　　　presence of peaks at 2θ values of 31.79°, 34.42°, 36.25°, 47.51°, 56.60°, 62.86°, 67.96° and

258　　　69.02° pointed out the formation of ZnO crystallites with hexagonal wurtzite structure, these

259　　　peaks corresponding to the lattice planes (100), (002), (101), (110), (103), (112) and (201),

260　　　respectively.

261

262　　**Figure 4**. XRD-patterns of selected Zn-catalysts supported on carbon supports and SBA-15.

263　　　The XPS analyses also confirm the formation of ZnO structures (Fig. 5). The spectral

264　　　regions of Zn $2p_{3/2}$ and $2p_{1/2}$, located at 1021.8 and 1045.2 eV, respectively, were fitted with

265 only a component (Fig. 5c and f). In previous studies, the Zn-O bonds have been assigned to

266 the peak at 1021.7 eV, while the signal corresponding to Zn-OH bonds in the hydroxide is

267 shifted to higher BE (1022.8 eV) [29]. All the carbon supports have a certain intrinsic oxygen

268 content forming different oxygenated surface groups denoted in the C1s spectra by different

269 contributions (Fig. 5a and d). In this case, the C1s peak was fitted using four components at

270 284.6 (C=C), 285.7 (C-O), 287.1 (C=O) and 289.9 eV (carbonate species). The analysis of the

271 O1s spectral region was fitted using three components, allowing to discriminate between the

272 oxygen linked to the carbon phase at 533.7 (C=O) and 532.3 (C-O), and the O-Zn bonds in the

273 crystal lattice at 531.1 eV (Fig 5b and e). The surface composition obtained from these

274 integrations denotes a higher Zn and O-contents on the Norit3Zn surface than on the $CNT_{ox}3Zn$

275 catalyst (Table 2). Because the theoretical Zn-content is similar in both samples, this result

276 points out a best accessibility of the surface Zn-structures formed on Norit AC. The total Zn

277 contents of both catalysts determined by XPS were similar, but the XPS analysis gives

278 information about the atomic concentration at the surface and it is dependent of (i) the

279 different sizes of Zn-particles and/or (ii) their different localization inside the porosity. It is

280 noteworthy that Norit3Zn and $CNT_{ox}3Zn$ presented similar Zn-contents determined by XPS,

281 but no XRD peaks were detected for $CNT_{ox}3Zn$ (Figure 4). This fact only indicates that Zn-

282 particles are not crystalline or they presented a very small size, and evidently, no information

283 related with the dispersion or nature of the Zn-phase can be analyzed from these results.
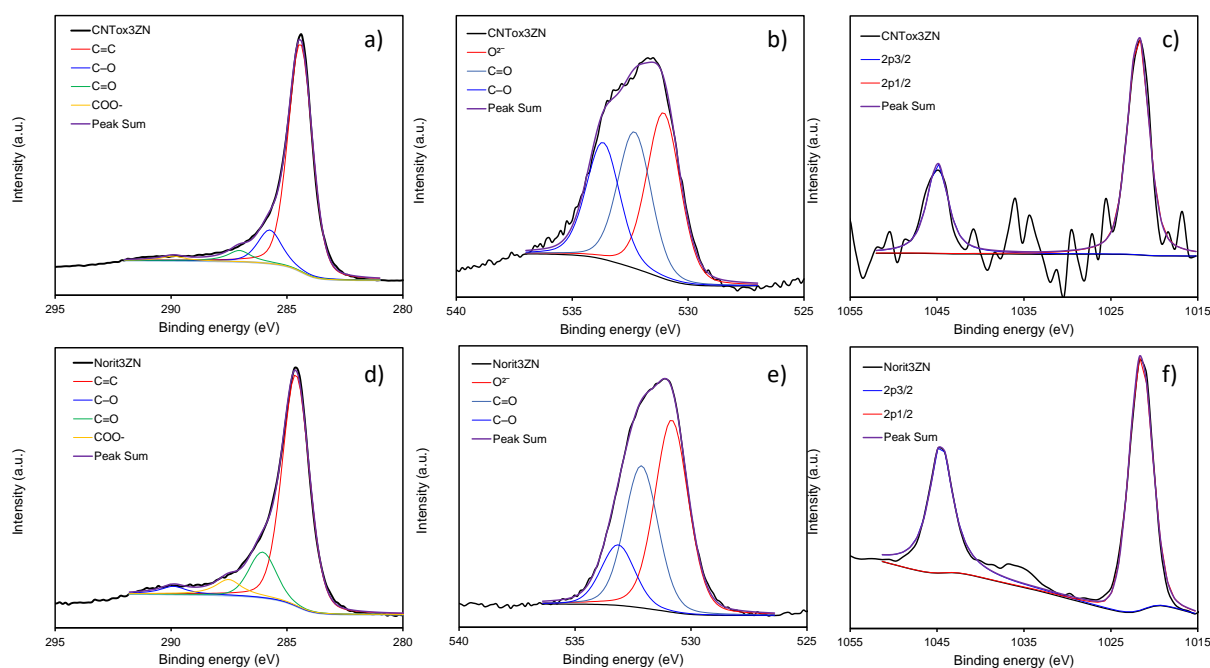
284

285

286

287

288　**Table 2.** Surface atomic composition, species percentage and corresponding binding energies

289　(in brackets, eV) of selected catalysts obtained by XPS.

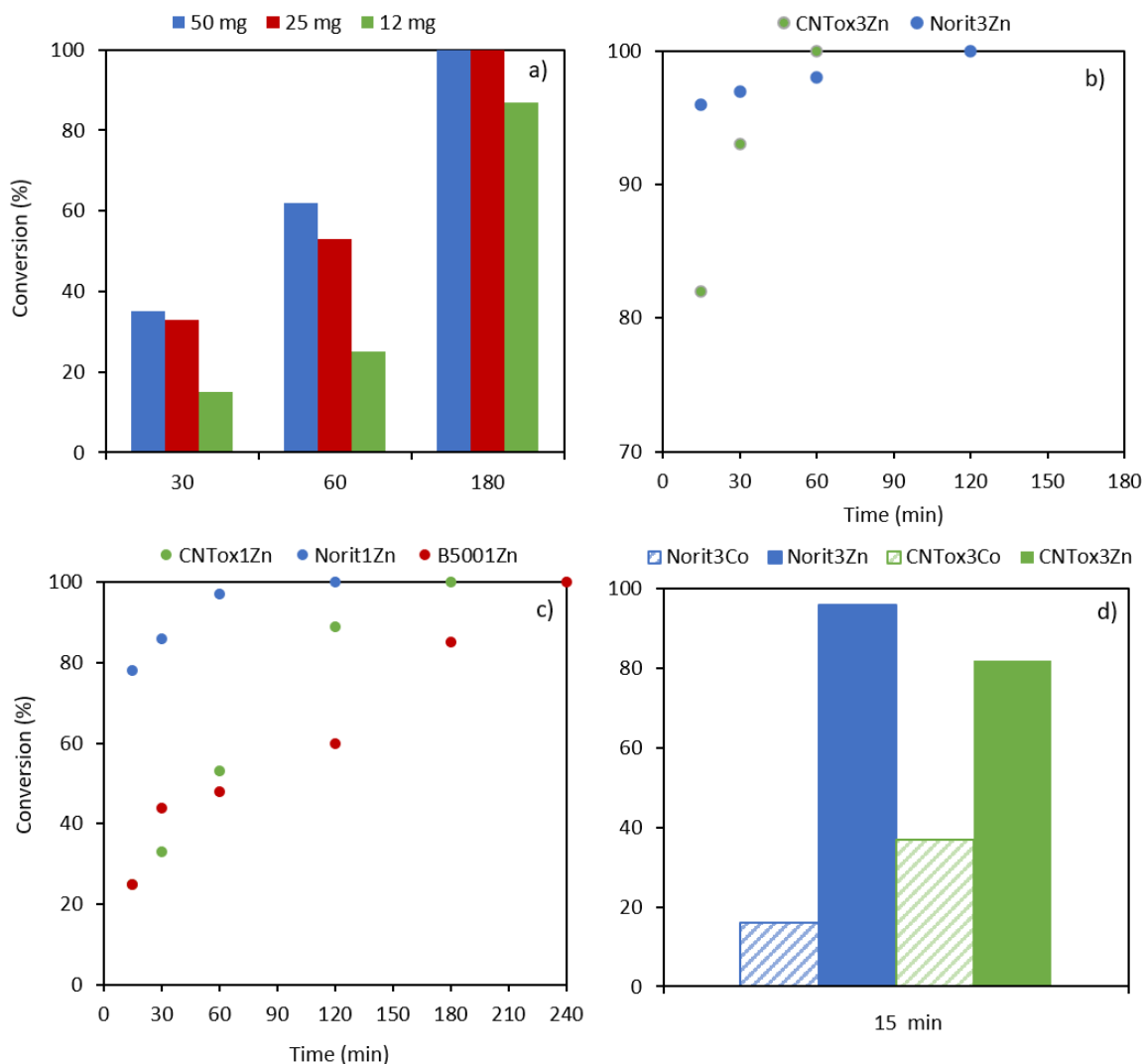|	C	O	Zn	C1s (%)				O1s (%)			Zn2p$_{3/2}$ (%)
	(%)	(%)	(%)	C=C	C–O	C=O	COO⁻	O^{2-}	C=O	C-O	ZnO
CNT$_{ox}$3Zn	75.9	21.7	2.5	80 (284.6)	13 (285.7)	5 (287.1)	2 (289.9)	40 (531.1)	32 (532.3)	28 (533.7)	100 (1021.7)
Norit3Zn	63.6	32.5	3.9	75 (284.6)	15 (285.9)	7 (287.3)	3 (289.7)	49 (531.0)	36 (532.3)	15 (533.3)	100 (1021.8)

290

291

292　**Figure 5**. XPS spectral and deconvolution of the (a, d) C1s region, (b, e) O1s region and (c, f)

293　Zn2p region for catalysts prepared with high Zn-loading.

294　*3.2. Catalytic performance*

295　　　The carbon catalysts under study were tested in the synthesis of quinolines **3a**, from 2-

296　amino-5-chlorobenzaldehyde **1a** and ethyl acetoacetate **2**, under solvent-free conditions, at
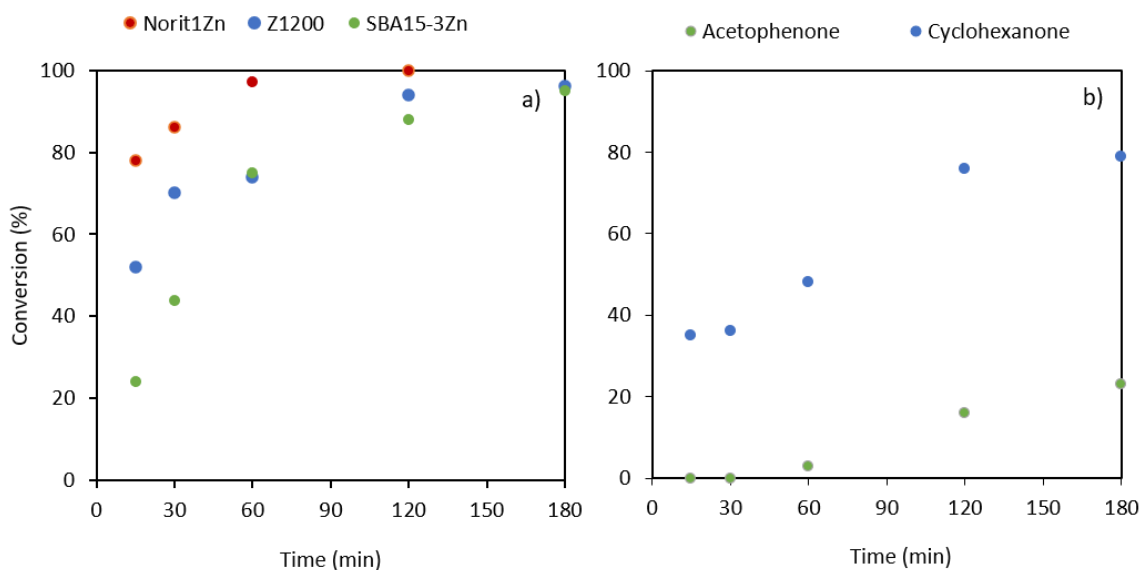
297　303 K (Scheme 1).

Figure 6. Synthesis of quinolines **3a** from 2-amino-5-chlorobenzaldehyde **1a** and ethyl acetoacetate **2** catalyzed by ZnO/carbon catalysts. a) Influence of the catalyst amount. b) ZnO/carbon catalysts with a theoretical Zn content of 3 wt.% and c) 1 wt.%. d) ZnO/carbon vs CoO/carbon catalysts.

The influence of the catalyst amount was firstly studied using the $CNT_{ox}1Zn$ catalyst; results are showed in Figure 6a. Conversion increased with the amount of the sample, but this increase is quite small when used 50 mg regarding the results obtained when using only with 25 mg. Then, we selected the optimum amount of the catalyst as 25 mg for further experiments. Figures 6b-c depict the conversion values *vs.* time obtained for the investigated

308 reaction catalyzed Zn-catalysts supported on the different carbon materials. It is noteworthy

309 that the carbon supports present a certain activity, approximately 20 % of conversion (after

310 2h) measured at 323 K (kinetics not shown), attributed to the presence of oxygenated surface

311 groups (OSG) as catalytic sites but also to π,π-stacking interactions between the catalyst

312 surface and aromatic reactant [30]. As expected, conversion increased with ZnO-loading and

313 depends on the ZnO concentration and the support nature, affording quinoline **3a** in almost

314 total conversions at short reaction times (96 % after only 15 min when used the Norit3Zn

315 catalysts). In the case of the samples with the lowest Zn loading, the conversion increased in

316 the sense $B_{500}1Zn$ < $CNT_{ox}1Zn$ < Norit1Zn (Fig. 6c), suggesting a negative effect of the

317 mesopores on the catalytic performance of this series. These results contrast with those

318 previously obtained [17] using CoO/carbon catalysts, where the activity of the catalysts is

319 favored using CNT as supports (Fig. 6d). Remarkably, ZnO/carbon samples show considerably

320 enhanced catalytic performance. The improved catalytic performance for the NoritYZn series

321 is clearly related with an optimized combination of porous and surface chemistry properties.

322 In particular, the Norit1Zn catalyst with the lowest Zn content yielded around 80 % of the

323 quinoline **3a** in only 15 min of reaction time (Fig. 6c), while for obtaining similar conversions

324 with $CNT_{ox}3Zn$ requires a superior Zn loading (Fig. 6b). Moreover, TEM analysis showed a

325 different morphology and localization of the Zn-structures. The narrower pore size

326 distribution of the Norit support can difficult the impregnation processes, Zn-precursor

327 remaining in a more external surface (as also denoted by XPS) and producing a fibrous coating

328 of the support particles. Thus, a faster reaction takes place on NoritYZn catalysts because the

329 higher Zn-content on surface with appropriate morphology and Zn-OH surface groups,

330 avoiding restrictions by diffusion process inside the mesoporosity of CNT_{ox} and specially, CA

331 B_{500}.

332   On the other hand, the hydroxylated surface on NoritYZn series could favor the presence

333 of water molecules weakly physisorbed [31,32]. Water plays an important role in numerous

334 applications, specifically water at surfaces in heterogeneous catalysis [33]. These effect has

335 been experimentally observed for amino-grafted metallosilicates catalyzing the Friedländer

336 reaction [34], but also when using $CaO/Ca(OH)_2$ supporting carbon materials as other example

337 [11,35]. The presence of water on Zn-containing catalysts could then stabilize transition

338 structures in different elementary steps concerning the synthesis of quinolines *via* Friedländer

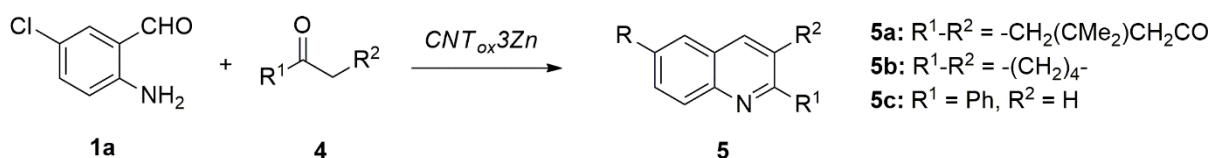339 reaction or chromene derivatives, as previously reported.

340   Given the extraordinary reactivity of investigated ZnO/carbon catalysts and considering

341 that the selection of the support is a key factor in the development of new catalysts with

342 improved properties, we also compared the performance of Norit1Zn, with other Zn-

343 containing catalysts such as a commercial MOF (Basolite® Z1200) or ZnO-supported on SBA-

344 15 mesoporous silica (SBA15-3Zn) (Fig. 7a). As observed, Norit1Zn is more active that both

345 alternative catalysts, in spite that they have a Zn-content around 3-fold higher. This behavior

346 is independent of the microporous character of the MOF, exhibiting even a greater

347 microporosity and surface area than AC Norit, the superior catalytic performance for NoritYZn

348 series probably related to the accessibility of active catalytic centers. The results obtained

349 when using the SBA15-3Zn sample, showing a homogeneous mesoporosity, are in good

350 agreement with those for mesoporous catalysts, $CNT_{ox}YZn$ and $B_{500}1Zn$, as previously

351 mentioned.

352

Figure 7. a) Synthesis of quinolines **3a** by Norit1Zn and alternative catalysts like Basolite®
Z1200 and SBA-15-3Zn. b) Synthesis of quinolines **5** catalyzed by $CNT_{ox}3Zn$, at 363 K under
solvent-free conditions.

This methodology has been applied to the synthesis of quinoline **5**, using other carbonyl
compounds (Scheme 2), in moderate to excellent conversions (24-99 %) in the presence of
$CNT_{ox}3Zn$ sample. The reaction in the presence of dimedone, at 353 K, led to the acridone **5a**
in quantitative conversions, in only 15 min of reaction time, whereas when using others less
reactive carbonyl components such as cyclohexanone and acetophenone, the corresponding
quinoline derivatives were obtained in 76 % (after 2h) and 24 % (after 3h), at 363K,
respectively (Fig. 7b).

Scheme 2. Synthesis of quinoline **5** catalyzed by $CNT_{ox}3Zn$, under solvent-free conditions.

4. Conclusions

21

366   In this work, we report for the first time new ZnO supporting carbon-based catalysts with

367   highly enhanced catalytic properties promoting the green and selective synthesis of quinoline

368   derivatives. The methodology reported herein is characterized by the use of easily prepared

369   Zn/carbon catalysts, which work under solvent-free and mild reaction conditions, to produce

370   poly-substituted quinolines and related compounds, in good to excellent conversions, through

371   cascade reactions with high atom economy, via Friedländer condensation. The catalysts are

372   prepared from the corresponding carbon support, by impregnation with $Zn(NO_3)_2 \cdot 6H_2O$

373   aqueous solutions, followed by thermal treatment. Zn loading in combination with porosity of

374   the samples and the accessibility of the catalytic sites are key factors determining the catalytic

375   performance and maximizing the metal efficiency. Our results demonstrate that the catalysts

376   reported herein represent an interesting and sustainable alternative to others structurally

377   different solid catalysts widely investigated in fine chemistry, such as metal-organic-

378   frameworks and mesoporous silicas.

386   **5.   References**

387   [1]   Y. K. Mishra, R. Adelung, ZnO tetrapod materials for functional applications, Mater.

388   Today 21, (2018) 631-651. https://doi.org/10.1016/j.mattod.2017.11.003

389   [2]   B. Banerjee, Recent developments on nano-ZnO catalyzed synthesis of bioactive

390   heterocycles, J. Nanostruct. Chem. 7 (2017) 389-413. https://doi.org/10.1007/s40097-

391   017-0247-0

392   [3]   L. Chen, H. Yu, J. Zhong, J. Wu, W. Su, Graphene based hybrid/composite for electron

393   field   emission: A   review,   J.   Alloys   Compds.   749   (2018)   60-84.

394   https://doi.org/10.1016/j.jallcom.2018.03.100

395   [4]   Y. Wang, X. Xiao, H. Xue, H. Pang, Zinc Oxide Based Composite Materials for Advanced

396   Supercapacitors,   *ChemistrySelect*   3   (2018)   550-565.

397   https://doi.org/10.1002/slct.201702780

398   [5]   J. Wang, T. Tsuzuki, B. Tang, X. Hou, L. Sun, X. Wang, Reduced Graphene Oxide/ZnO

399   Composite: Reusable Adsorbent for Pollutant Management, ACS Appl. Mater. Interfaces

400   4 (2012) 3084-3090. https://doi.org/10.1021/am300445f

401   [6]   U.C. Rajesh, J. Wang, S.W. Prescott, T. Tsuzuki, D.S. Rawat, RGO/ZnO Nanocomposite:

402   An Efficient, Sustainable, Heterogeneous, Amphiphilic Catalyst for Synthesis of 3-

403   Substituted   Indoles   in   Water,   ACS   Sustain.   Chem.   Eng.   3   (2015)   9-18.

404   https://doi.org/10.1021/sc500594w

405   [7]   T. Krithiga, S. Salla, J. Karthikeyan, J. A. Kumar, One-pot Synthesis of beta-acetamido-

406   beta-(phenyl) Propiophenone using ZnO/Carbon Nanocomposites, Comb. Chem. High

407   Throughput Screen 24 (2021) 213-219. DOI 10.2174/1386207323666200606213536

408   [8]   B. Chen, C. Zhang, L. B. Niu, X. Z. Shi, H. L. Zhang, X. W. Lan, G. Y. Bai, Biomass-Derived

409   N-doped Carbon Materials with Silica-Supported Ultrasmall ZnO Nanoparticles: Robust

410   Catalysts for the Green Synthesis of Benzimidazoles, Chem. Eur. J. 24 (2018) 3481-3487.

411   DOI 10.1002/chem.201704823

412   [9]   Z.H. Yu, H.-F. Zheng, W. Yuan, Z. L. Tang, A.-D. Zhang, D.-Q. Shi, An unexpected one-pot

413   synthesis of multi-substituted quinolines via a cascade reaction of

414   Michael/Staudinger/aza-Wittig/aromatization of ortho-azido-b-nitro-styrenes with

415   various carbonyl compounds, Tetrahedron 69 (2013) 8137-8141.

416   http://dx.doi.org/10.1016/j.tet.2013.07.050

417   [10]   H. Jiang, X. An, K. Tong, T. Zheng, Y. Zhang, S. Yu, Visible-Light-Promoted Iminyl-Radical

418   Formation from Acyl Oximes: A Unified Approach to Pyridines, Quinolines, and

419   Phenanthridines, Angew. Chem. 127 (2015) 4127–4131. DOI: 10.1002/anie.201411342

420   [11]   J. Marco-Contelles, E. Pérez-Mayoral, A. Samadi, M.C. Carreiras, E. Soriano, Recent

421   Advances in the Friedländer Reaction, Chem. Rev. 109 (2009) 2652-2671.

422   https://doi.org/10.1021/cr800482c

423   [12]   J. M. Muchowski, M. L. Maddox, Concerning the mechanism of the Friedländer

424   quinoline synthesis, Can. J. Chem. 82 (2004) 461–478. doi: 10.1139/V03-211

425   [13]   A. Mai, D. Rotili, D. Tarantino, P. Ornaghi, F. Tosi, C. Vicidomini, G. Sbardella, A.

426   Nebbioso, M. Miceli, L. Altucci, P. Filetici, Small-Molecule Inhibitors of Histone

427   Acetyltransferase Activity: Identification and Biological Properties, J. Med. Chem. 49

428   (2006) 6897–6907. https://doi.org/10.1021/jm060601m

429

430   [14]   A.T. Smith, M.R. Livingston, A. Mai, P. Filetici, S.F. Queener, W.J. Sullivan, Quinoline

431   Derivative MC1626, a Putative GCN5 Histone Acetyltransferase (HAT) Inhibitor, Exhibits

432   HAT-Independent Activity against Toxoplasma gondii, Antimicrob. Agents Chemother.

433   51 (2007) 1109–1111. DOI: 10.1128/AAC.01256-06

434   [15]   A. Nourry, S. Legoupy, F. Huet, Synthesis of an analogue of lavendamycin and of

435   conformationally restricted derivatives by cyclization via a hemiaminal intermediate,

436   Tetrahedron Lett. 48 (2007) 6014–6018. DOI: 10.1016/j.tetlet.2007.06.100

437   [16]   M. Godino-Ojer, A. J. López Peinado, F. J. Maldonado-Hódar, E. Pérez-Mayoral, Highly

438   Efficient and Selective Catalytic Synthesis of Quinolines Involving Transition-Metal-

439   Doped   Carbon   Aerogels,   ChemCatChem   9   (2017)   1422-1428.

440   https://doi.org/10.1002/cctc.201601657

441   [17]   M. Godino-Ojer, A. J. López-Peinado, F. J. Maldonado-Hódar, E. Bailón-García, E. Pérez-

442   Mayoral, Cobalt oxide–carbon nanocatalysts with highly enhanced catalytic

443   performance for the green synthesis of nitrogen heterocycles through the Friedländer

444   condensation,   Dalton   Trans.   48   (2019)   5637-5648.

445   https://doi.org/10.1039/C8DT04403A

446   [18]   L. Leyssens, B. Vinck, C. Van Der Straeten, F. Wuyts, L. Maes, Cobalt toxicity in humans-

447   A review of the potential sources and systemic health effects, Toxicology 387 (2017) 43-

448   56. https://doi.org/10.1016/j.tox.2017.05.015

449   [19]   F. J. Maldonado-Hódar, Advances in the development of nanostructured catalysts based

450   on   carbon   gels,   Catal.   Today   218   (2013)   43-50.

451   https://doi.org/10.1016/j.cattod.2013.06.005

452 [20] M. Trépanier, A. Tavasoli, A. K. Dalai, N. Abatzoglou, Co, Ru and K loadings effects on the

453 activity and selectivity of carbon nanotubes supported cobalt catalyst in Fischer–Tropsch

454 synthesis, Appl. Catal. A 353 (2009) 193–202. DOI 10.1016/j.apcata.2008.10.061.

455 [21] J. López-Sanz, E. Pérez-Mayoral, E. Soriano, M. Sturm, R. M. Martín-Aranda, A. J. López-

456 Peinado, J. Čejka, New inorganic–organic hybrid materials based on SBA-15 molecular

457 sieves involved in the quinolines synthesis, Catal. Today 187 (2012) 97-103.

458 https://doi.org/10.1016/j.cattod.2011.12.015

459 [22] M. M. Dubinin, in Chemistry and Physics of Carbon, P. L. Walker Jr., Marcel Dekker (Eds),

460 New York, 1966, 51.

461 [23] F. Duarte, F. J. Maldonado-Hodar, L. M. Madeira, Influence of the characteristics of

462 carbon materials on their behaviour as heterogeneous Fenton catalysts for the

463 elimination of the azo dye Orange II from aqueous solutions, Appl. Catal. B 10 (2011)

464 109-115. https://doi.org/10.1016/j.apcatb.2011.01.016

465 [24] Z.-H. Yu, H.-F. Zheng, W. Yuan, Z.-L. Tang, A.-D. Zhang, D.-Q. Shi, An unexpected one-pot

466 synthesis of multi-substituted quinolines via a cascade reaction of

467 Michael/Staudinger/aza-Wittig/aromatization of ortho-azido-⍰-nitro-styrenes with

468 various carbonyl compounds, Tetrahedron 69 (2013) 8137-8141.

469 https://doi.org/10.1016/j.tet.2013.07.050

470 [25] T. Xu, Y. Shao, L. Dai, S. Yu, T. Cheng, J. Chen, Pd-Catalyzed Tandem Reaction of 2-

471 Aminostyryl Nitriles with Arylboronic Acids: Synthesis of 2-Arylquinolines, J. Org. Chem.

472 84 (2019) 13604–13614. https://doi.org/10.1021/acs.joc.9b01875

473 [26] M. Godino-Ojer, I. Matos, M. Bernardo, R. Carvalho, O. S. G.P. Soares, C. Durán-Valle,

474 I.M. Fonseca, E. Pérez Mayoral, Acidic porous carbons involved in the green and

475   selective synthesis of benzodiazepines, Catal. Today 357 (2020) 64–73.

476   https://doi.org/10.1016/j.cattod.2019.11.027

477   [27] M. Godino-Ojer, L. Milla-Diez, I. Matos, C. J. Durán-Valle, M. Bernardo, I. M. Fonseca, E.

478   Pérez Mayoral, Enhanced Catalytic Properties of Carbon supported Zirconia and Sulfated

479   Zirconia for the Green Synthesis of Benzodiazepines, ChemCatChem 10 (2018) 5215-

480   5223. DOI:10.1002/cctc.201801274

481   [28] E. Gallegos-Suárez, A. F. Pérez-Cadenas, F. J. Maldonado-Hódar, F. Carrasco-Marín, On

482   the micro- and mesoporosity of carbon aerogels and xerogels. The role of the drying

483   conditions during the synthesis processes, Chem. Eng. J. 181-182 (2012) 851-855.

484   https://doi.org/10.1016/j.cej.2011.12.002

485   [29] S. B. Amor, M. Jacquet, P. Fioux, M. Nardin, XPS characterisation of plasma treated and

486   zinc oxide coated PET, Appl. Surf. Sci. 255 (2009) 5052-5061.

487   https://doi.org/10.1016/j.apsusc.2008.12.067

488   [30] M. Godino-Ojer, E. Soriano, V. Calvino-Casilda, F. J. Maldonado-Hódar, E. Pérez Mayoral,

489   Metal-free synthesis of quinolines catalyzed by carbon aerogels: Influence of the porous

490   texture and surface chemistry, Chem. Eng. J. 314 (2017) 488-497.

491   https://doi.org/10.1016/j.cej.2016.12.006

492   [31] M. Nagao, On Physisorption of Water on Zinc Oxide Surface, J. Phys. Chem. 75 (1971)

493   3822–3828. https://doi.org/10.1021/j100694a007

494   [32] V. Quaranta, J. Behler, M. Hellström, Structure and Dynamics of the Liquid−Water/Zinc-

495   Oxide Interface from Machine Learning Potential Simulations, J. Phys. Chem. C 123

496   (2019) 1293–1304. https://doi.org/10.1021/acs.jpcc.8b10781

497   [33] P. R. Davies, On the Role of Water in Heterogeneous Catalysis: A Tribute to Professor M.

498   Wyn Roberts, Top. Catal. 59 (2016) 671-677. https://doi.org/10.1007/s11244-016-0539-

499   5

500   [34] A. Smuszkiewicz, J. López-Sanz, E. Pérez-Mayoral, E. Soriano, I. Sobczak, M. Ziolek, R. M.

501   Martín-Aranda, A.J. López-Peinado, Amino-grafted mesoporous materials based on MCF

502   structure involved in the quinoline synthesis. Mechanistic insights, J. Mol. Catal. A 378

503   (2013) 38-46. https://doi.org/10.1016/j.molcata.2013.05.017

504   [35] D. González-Rodal, J. Przepiórski, A. J. López Peinado, E. Pérez-Mayoral, Basic-carbon

505   nanocatalysts in the efficient synthesis of chromene derivatives. Valorization of both PET

506   residues and mineral sources, Chem. Eng. J. 382 (2020) 122795.

507   https://doi.org/10.1016/j.cej.2019.122795

508

509